Journal of Sound and Vibration (1997) **207**(4), 567–589

DYNAMICS OF A TWO-LINK FLEXIBLE SYSTEM UNDERGOING LOCKING: MATHEMATICAL MODELLING AND COMPARISON WITH EXPERIMENTS

B. P. Nagaraj and B. S. Nataraju

Dynamics and Analysis Division, Spacecraft Mechanism Group, ISRO Satellite Centre, Airport Road, Vimanapura P.O., Bangalore 560 017, *India*

and

A. Ghosal

Department of Mechanical Engineering, Indian Institute of Science, Bangalore 560 012, *India*

(*Received* 8 *August* 1996, *and in final form* 18 *June* 1997)

Space structures such as the solar panels or antenna, when deployed in space, have large dimensions, low mass to size ratio, large inertias and relatively low structural rigidity. Due to space restrictions, these structures are originally in stowed configurations and are deployed into their full size in space. Typically, these systems at the end of deployment undergo locking at the joints and lose their rotational degrees of freedom at the joints. In addition, during locking vibrations are induced in these light-weight, flexible mechanisms which have to be actively or passively damped. In this paper a mathematical model with an experiment is presented for a two-link flexible system, which undergoes locking during motion. The structural flexibility is modelled by the finite element method, and the equations of motion are derived using the Lagrangian formulation. The locking at the joints is modelled by the momentum balance method, which enables one to predict the rigid body as well as the elastic motion of the system after locking. The experimental setup consists of two flexible aluminum links with a revolute joint at the end of each link, and has a locking mechanism for each joint. The links lock at a predefined angle. The links are instrumented with strain gages and the joint rotations are measured by potentiometers. The sensor readings are acquired and stored on a PC based data acquisition system. The simulation results such as the locking time, response of each joint and the strain at the base of each link match very well with the experimental results. Thus, the momentum balance method is capable of predicting fairly accurately the dynamics of a flexible system which undergo locking during motion.

1. INTRODUCTION

Future structures deployed in space and platforms to be assembled in space will have large dimensions. The weight of these space structures needs to be as small as possible, and hence, the structures designed will have relatively low structural rigidity. In addition, the volume limitations inside the fairing of launch vehicles, as well as high launch loads, have necessitated the design of many structures (for example deployable solar arrays and antennae) in a compact stowed manner during the launch and mechanisms [1] to deploy them in space. The dynamics modelling of these structures including flexibility helps to predict the accurate response of the system during deployment.

0022–460X/97/440567 + 23 $25.00/0/sv971194

Many mechanical systems are subjected to changes in kinematic structure during their functional use. One common example is the locking of individual solar arrays of a satellite during deployment. This operation results in a redistribution of total momentum that may lead to impulsive forces and moments on the system. These impulsive forces may lead to large vibrations in the lightweight flexible structures and may also cause damage to the mechanical components.

A large number of researchers have developed mathematical models and numerical simulation tools for studying the structural flexibility of the members during their motion. The flexibility is modelled by the finite element method in [2–5], assumed mode method [5–8] and lumped parameter approach [9].

In the finite element method, an elastic member is approximated as a number of discrete (finite) elements with the nodes having translational and rotational degrees of freedom. The deflection in between nodes is approximated by polynomial shape functions. In the assumed mode method the link flexibility is represented by the finite number of modes, in terms of spatial eigenfunctions which are transcendental and time dependent mode amplitudes. In the lumped parameter approach each link is discretised into a smaller number of elements having mass and stiffness in the form of springs.

The deployment analysis of accordion type of solar array, stowed during launch and deployed in orbit, is discussed in [10–11] with the links assumed to be rigid bodies. This is not strictly correct since these structures are flexible and there can be significant vibration induced due to locking. Several researchers have studied the post impact behavior of closed loop mechanisms and a single flexible link, and validated numerical simulation with the experimental results. Khulief and Shabana [12] used momentum balance method for constrained mechanical systems with interconnected rigid and flexible bodies. The joints between different components are introduced in the dynamic equations using constraint equations and Lagrange multiplier technique. The intermittent motion is monitored by an event predictor algorithm. The authors extended their theory in [13] to a general multibody system subject to kinematic structure changes during motion. Rasmentab-Sany and Shabana [14] used the above method for a radially rotating flexible beam with an axial impact. The deformation of the beam in the axial direction is described using Fourier series. The momentum balance method is used by Yigit [15] for a radially rotating beam impacting on a horizontal surface. In the previous investigations [12–14] the applicability of coefficient of restitution for flexible systems was not addressed. Yigit *et al*. in [16] validated the analyticaly developed impact model through experiment. The strain gages were used to measure the elastic deformation and angular velocity was measured by an optical encoder. They compared the angular velocity and strain along the beam with analytical and experimental results. From these comparisons, they concluded that the momentum balance method can be used to predict the post dynamic behavior of similar systems with good accuracy. In [17], the authors studied the impact of a radially rotating beam with a spring dashpot model. The spring model is based on non-linear force displacement relationships based on Hertzian contact. The results were found to be in good agreement with experiment.

The impact of a sphere on a single elastic flexible robot arm is investigated by Chapnick *et al*. [18]. The elastic motion of the link was measured through photo detector diode and the joint angle was measured by an optical encoder. The simulation results are also compared with experimental data. The contact phenomenon during impact is modelled based on Hertzian theory of contact. The coefficient of restitution is calculated based on the energy absorbed from impact by each mode of vibration. The impact of a rigid–flexible manipulator impacting on a rigid spherical surface is investigated by Yigit [19]. The impact is modelled by a spring dashpot model based on the Hertzian contact law. Hence, the

impact behaviour can be modelled by a spring dashpot model or momentum balance method. The spring dashpot model requires additional parameters to be determined, as it is based on the relative indentation and damping. The change in velocity of the system after impact is obtained by appending the spring dashpot model to the differential equation of motion. The momentum balance method is derived based on the integration of the equations of motion over the impact period and on the coefficient of restitution. This results in a set of linear algebraic equations which can be solved to compute the change in velocity after impact.

Based on the above literature survey, there is no available literature on the analysis of flexible systems which undergo locking at the joints during motion. In this paper a mathematical model and experimental setup is presented for a flexible two-link (revolute joints) system which undergo locking during motion. The theory developed here is helpful in the analysis of the deployment dynamics of a 2R (revolute) flexible link (simulating a two-element solar array or antenna) which undergoes locking during motion. Finally, the experimental results will be compared with the simulation in order to assess the validity of the mathematical model. The paper is organised as follows: In section 2, a brief description of the system is presented. The equations of motions for the flexible two link system is presented in section 3. The mathematical model for locking at the joints using the momentum balance method is presented in section 4. The equations of motion for the single flexible link after first locking is presented in section 5. Numerical simulation results are presented in section 6. In section 7 the experimental set up is described. The description of major components are presented in section 8. The instrumentation used in the experimental set-up is described in section 9. In section 10, the experimental results are presented and compared with numerical simulation. Finally the concluding remarks are presented in section 11.

2. SYSTEM DESCRIPTION AND MODELLING

The schematic representation of the two-link flexible system is shown in Figure 1(a). The links are supported by air bearings at the end and the motions of the links is on a flat horizontal table. This arrangement ensures that gravity effects can be neglected. The two flexible links are initially folded with a known initial angle and released from the initial configuration. Each link is actuated by means of pre-loaded torsion spring mounted at the joints. The initial motion of the link is indicated by the arrows in the Figure 1(b). The first stage of locking takes place, when the angle between first link and the second link is zero, as shown in Figure 1(c). After the first locking the second joint loses its rotational degree of freedom and the system now rotates about the first joint, like a single flexible

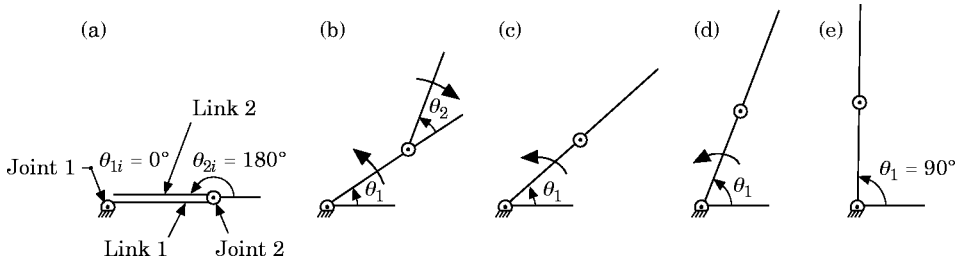

Figure 1. Schematic representation of motion of two-link flexible system. (a) Initial configuration; (b) Intermediate configuration; (c) First stage of locking; (d) Motion after first stage of locking; (e) Second stage of locking.

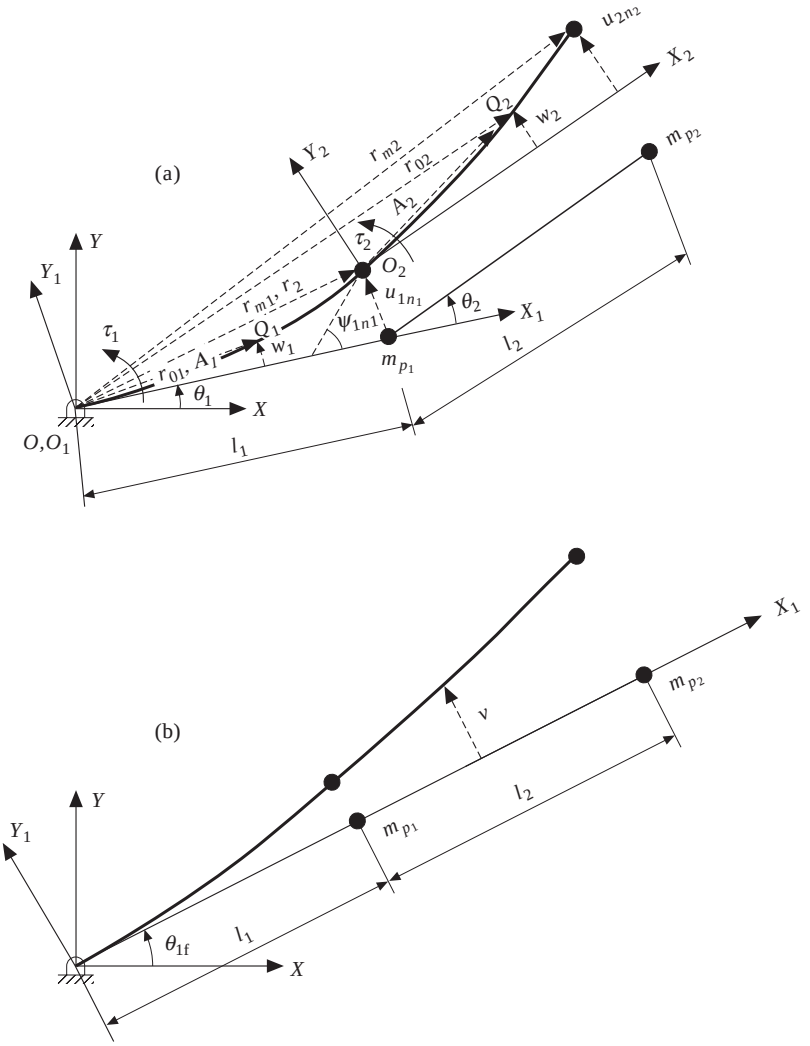

Figure 2. Schematic representation. ═══, deformed shape; ——, original shape; ----, position vectors; (a) two-link flexible system; (b) single flexible link.

link as shown in Figure 1(d). A second locking takes place, when the first link rotates through 90° as shown in Figure 1(e). After the second locking the first joint loses its rotational degree of freedom, and the system behaves as a cantilever beam clamped about the first joint.

The schematic representation of a two-link flexible system is shown in Figure 2(a) with the original and the deformed configuration. The co-ordinate system OXY is the inertial reference frame. The body fixed co-ordinate system $O_i X_i Y_i$ is attached to the link i with origin at O_i with X_i-axis along the link i. The flexural deformation is described relative to the co-ordinate system that follows the rigid body motion of link.

The following assumptions are made in the mathematical formulation.

1. Each link is considered to have a constant cross sectional area and uniform material properties.

2. Each link is subjected to pure bending. The experimental configuration is designed to eliminate the possibility of torsion of the beam, and the torsional effects are neglected.

3. The motion of the flexible two-link system under study can have deformation only in the horizontal plane. Each link is supported on the air bearing. Hence, the bending due to gravity is negligible.

4. The beam is long and slender. The transverse shear and rotary inertia effects are negligible. This allows the use of Euler–Bernoulli beam theory to model the elastic deformation.

5. The stress induced due to the motion of link is well within the elastic limit.

The flexural deformation of a link is approximated by means of the finite element method [20]. The first link has n_1 elements and the second link has n_2 elements. The local displacement w_i of link i is expressed as a linear combination of shape functions $\mathbf{N}$ and the nodal degrees of freedom $\mathbf{d}_{in}$ as

$$w_i = \mathbf{N}\mathbf{d}_{in}. \tag{1}$$

The nodal degree of freedom, $\mathbf{d}_{in}$ for nth element of link i is given by

$$\mathbf{d}_{in} = \{u_{i(n-1)}, \psi_{i(n-1)}, u_{in}, \psi_{in}\}^{\mathrm{T}}, \tag{2}$$

where $u_{i(n-1)}$, u_{in} are the translational degrees of freedom for the nth element of link i and $\psi_{i(n-1)}$, ψ_{in} are the rotational degrees of freedom for the nth element of link i.

With the assumptions of a Euler–Bernoulli beam, the Hermite cubic shape functions for the beam element in the interval (0, 1) are given by

$$\phi_1(s) = 1 - 3s^2 + 2s^3, \qquad \phi_2(s) = l_{ie}(s - 2s^2 + s^3), \qquad \phi_3(s) = 3s^2 - 2s^3,$$
$$\phi_4(s) = l_{ie}(s^3 - s^2), \tag{3}$$

where $s = x_i / l_{ie}$, and x_i is the local co-ordinate of the element on link i. In the above equation l_{ie} is the length of the element of link i with $l_{ie} = l_i / n_i$ where l_i is the link length of link i and n_i is the number of elements on link i.

The shape function vector $\mathbf{N}$ is given by

$$\mathbf{N} = \{\phi_1(s), \phi_2(s), \phi_3(s), \phi_4(s)\}. \tag{4}$$

3. DYNAMIC EQUATIONS OF A FLEXIBLE TWO-LINK SYSTEM

The vector $\mathbf{r}_i$ locates the position of the origin of local (O_i, X_i, Y_i) co-ordinate system of link i in the reference frame. The vector $\mathbf{A}_i$ presents the co-ordinates of elastic deformation of link i with respect to the (O_i, X_i, Y_i). The vector $\mathbf{r}_{oi}$ measures the location with respect to the inertial co-ordinate system.

The position vector $\mathbf{r}_{oi}$ of any point Q_i on the link i from the origin of inertial frame is given by

$$\mathbf{r}_{oi} = \mathbf{r}_i + \mathbf{T}_i \mathbf{A}_i \tag{5}$$

where, $\mathbf{r}_1$ is $\{\mathbf{0}\}$ for link 1, $\mathbf{A}_i$ is given by $\{x_i, w_i\}^{\mathrm{T}}$, $\mathbf{r}_2$ is given as $\mathbf{T}_1 \mathbf{C}_1$ with $\mathbf{C}_1$ given as $\{l_1, u_{1n_1}\}^{\mathrm{T}}$, and

$$[T]_i = \begin{bmatrix} \cos(f_i) & -\sin(f_i) \\ \sin(f_i) & \cos(f_i) \end{bmatrix}.$$

In the above equations, $\mathbf{A}_i$ is the co-ordinate of point Q_i in the body fixed co-ordinate system, x_i is the horizontal distance, w_i is the flexural deformation of link i in the body

fixed co-ordinate system, $\mathbf{T}_i$ is the tranformation matrix relating to the body fixed and the inertial frame and f_i is the rotation of the joint i with respect to the inertial frame. f_1 is θ_1 for link 1, f_2 is $(\theta_1 + \theta_2 + \psi_{1n_1})$ for link 2, u_{in_i} is the tip displacement of link i, ψ_{1n_1} is the tip slope of link 1 and n_i is the number of elements on link i.

The position vector $\mathbf{r}_{mi}$ of the tip mass, m_{pi}, of link i is given by

$$\mathbf{r}_{mi} = \mathbf{r}_i + \mathbf{T}_i \, \mathbf{C}_i, \tag{6}$$

where $\mathbf{C}_2$ is given by $\{(l_1 + l_2), u_{2n_2}\}^{\mathrm{T}}$.

3.1. KINETIC ENERGY

From the position vectors, one can now find the kinetic energy [4, 21] of the two-link system. The total kinetic energy of the flexible system is due to the motion of the links and joints, and kinetic energy due to the tip mass.

3.1.1. *Kinetic energy of link i*

The kinetic energy T_{in} of the nth element of link i is given by

$$T_{in} = \tfrac{1}{2} \int_0^{l_{ie}} \rho_i \, A_i \left[\frac{\mathrm{d}\mathbf{r}_{0i}}{\mathrm{d}t}\right]^{\mathrm{T}} \cdot \left[\frac{\mathrm{d}\mathbf{r}_{0i}}{\mathrm{d}t}\right] \mathrm{d}x_i, \tag{7}$$

where ρ_i is the density, A_i is the cross-sectional area, l_{ie} is the length of an element and $\mathbf{r}_{oi}$ is the position vector of point Q_i on link i (refer to equation (5)).

As the link i is divided into n_i elements, the total kinetic energy T_i of a link is obtained by summing over all the elements of the link as follows:

$$T_i = \sum_{n=1}^{n_i} T_{in}. \tag{8}$$

3.1.2. *Kinetic energy of revolute joint i*

The joint inertia at the first joint is due to the joint assembly, and the joint inertia at the second joint is due to the joint assembly and the air bearing mounted at the second joint.

The kinetic energy for the joint i is given by

$$T_{J_i} = \tfrac{1}{2} \, \Omega_i^{\mathrm{T}} \, [J_i] \Omega_i, \tag{9}$$

where Ω_i is the angular velocity and J_i is the joint inertia of the joint i.

3.1.3. *Kinetic energy of the tip mass of link i*

The mass located at the tip of link 1 is the mass of associated mechanism of joint 2. The mass located at the tip of link 2 is the mass of the air bearing mounted at the tip of link 2.

The kinetic energy T_{mi} of the tip mass m_{pi} located at the tip of link i is given by

$$T_{mi} = \tfrac{1}{2} \, m_{pi} \left[\frac{\mathrm{d}\mathbf{r}_{mi}}{\mathrm{d}t}\right]^{\mathrm{T}} \cdot \left[\frac{\mathrm{d}\mathbf{r}_{mi}}{\mathrm{d}t}\right], \tag{10}$$

where $\mathbf{r}_{mi}$ is the position vector of the tip mass (refer to equation (6)).

The total kinetic energy of the system is given by

$$T = \sum_{i=1}^{2} (T_i + T_{Ji} + T_{mi}), \tag{11}$$

where i is the number of links in the system.

Substituting equations (1)–(4) and the derivative of equations (5) and (6) in the above equation, the total kinetic energy can be written in a compact form as

$$T = \tfrac{1}{2} \{\dot{\mathbf{q}}\}^{\mathrm{T}} [\mathbf{M}] \{\dot{\mathbf{q}}\} \tag{12}$$

where

$$\{\mathbf{q}\} = \{\theta_1, \theta_2, \mathbf{q}_1, \mathbf{q}_2\}^{\mathrm{T}}.$$

In the above equations, θ_1 and θ_2 are the joint rotations, and $\mathbf{q}_1$ and $\mathbf{q}_2$ are the nodal degrees of freedom of each link. These are given for $\mathbf{q}_i$, as $\{u_{i0}, \psi_{i0}, \ldots, u_{in_i}, \psi_{in_i}\}^{\mathrm{T}}$ and [**M**] is the mass matrix of the system.

3.2. POTENTIAL ENERGY

The potential energy of the flexible system arises from two sources: the strain energy due to the elastic deformation of the links [4, 21] and the potential energy of the torsion springs mounted at the joints.

3.2.1. *Potential energy of link i*

The strain energy V_{in} for the nth element of link i is given by

$$V_{in} = \tfrac{1}{2} \int_0^{l_{ie}} E_i I_i \left[\frac{\mathrm{d}^2 w_i}{\mathrm{d}x_i^2}\right]^{\mathrm{T}} \cdot \left[\frac{\mathrm{d}^2 w_i}{\mathrm{d}x_i^2}\right] \mathrm{d}x_i, \tag{13}$$

where E_i is Young's modulus, I_i is the area moment of inertia, w_i is the flexural deformation (refer equation (1)) of link i and l_{ie} is the length of the beam element of link i. The total strain energy, V_i is computed by summing over all the elements n_i of link i and can be written in a compact form as

$$V_i = \sum_{n=1}^{n_i} V_{in}. \tag{14}$$

3.2.2. *Potential energy of torsion springs*

The potential energy, V_s, due to the torsion spring at the ith joint by

$$V_s = \sum_{i=1}^{n_j} \tfrac{1}{2} K_{si} (\theta_{i0} - \theta_i)^2, \tag{15}$$

where K_{si} is the torsion spring stiffness of the joint i, θ_{i0} is the pre-rotation angle of joint i, θ_i is the joint angle, and n_j is the number of joints of the system and is equal to 2.

The total potential energy, V, of the system is given by

$$V = V_s + \sum_{i=1}^{2} V_i. \tag{16}$$

The above equation after simplification can be written as

$$V = \tfrac{1}{2}\{\mathbf{q}\}^{\mathrm{T}}[\mathbf{K}]\{\mathbf{q}\}, \tag{17}$$

where [**K**] is the flexural stiffness matrix.

3.2.3. *Torque due to rocker arm*

The torque τ_i acting at each joint due to the spring force exerted by the rocker arm on the cam mounted at each joint is computed by the principle of virtual work. The torque is related to the virtual work, δW_t, by

$$\delta W_t = \sum_{i=1}^{n_j} \tau_i \, \delta\theta_i, \tag{18}$$

where the infinitesimal displacements of each joint is $\delta\theta_i$.

3.3. BOUNDARY CONDITIONS

The first joint has only a rotational degree of freedom θ_1 with respect to the inertial axis OX. This contrains the nodal degree of freedom corresponding to the first element attached to the joint O_1. Hence one gets

$$u_{10} = 0 \qquad \text{and} \qquad \psi_{10} = 0 \qquad \text{at} \qquad x_1 = 0. \tag{19}$$

The second joint has only one rotational degree of freedom relative to the first link. Thus the constraints for the second link are

$$u_{20} = 0 \qquad \text{and} \qquad \psi_{20} = 0 \qquad \text{at} \qquad x_2 = 0. \tag{20}$$

3.4. EQUATIONS OF MOTION FOR A TWO-LINK SYSTEM

The equations of motion are derived based on the Lagrangian formulation [22]. The Lagrangian of the system in terms of the generalised coordinates $\mathbf{q}$ and its derivative $\dot{\mathbf{q}}$ is given by

$$L(\mathbf{q}, \dot{\mathbf{q}}) = T - V, \tag{21}$$

where T and V are the total kinetic and potential energies of the system. The equations of motion are obtained from the Lagrangian by using

$$\mathrm{d}/\mathrm{d}t(\partial L(\mathbf{q}, \dot{\mathbf{q}})/\partial\dot{\mathbf{q}}) - \partial L(\mathbf{q}, \dot{\mathbf{q}})/\partial\mathbf{q} = \tau. \tag{22}$$

The equations of motion can be written in a compact matrix form as

$$\begin{bmatrix} M_r & M_{rf} \\ M_{rf}^{\mathrm{T}} & M_f \end{bmatrix} \begin{Bmatrix} \ddot{\mathbf{q}}_r \\ \ddot{\mathbf{q}}_f \end{Bmatrix} + \begin{Bmatrix} h_r(\mathbf{q}, \dot{\mathbf{q}}) \\ h_f(\mathbf{q}, \dot{\mathbf{q}}) \end{Bmatrix} + \begin{bmatrix} K_j & 0 \\ 0 & K_f \end{bmatrix} \begin{Bmatrix} \mathbf{q}_r \\ \mathbf{q}_f \end{Bmatrix} = \begin{Bmatrix} \tau \\ 0 \end{Bmatrix} \tag{23}$$

The first term contains the configuration dependent mass matrix and the second derivative of the generalised co-ordinates. This matrix can be separated into the matrix containing rigid body terms (M_r), the matrix containing terms involving the coupling of the rigid body and flexible variables (M_{rf}), and the matrix containing the terms involving only the flexible variables (M_f). The generalised coordinates $\mathbf{q}_r$ are the joint rotations θ_1 and θ_2 respectively and $\mathbf{q}_f$ are the nodal degrees of freedom of each link. The second term is the vector of Coriolis and centripetal terms. The third term is the stiffness term and this can be separated into contributions from the torsion spring and the links. The term on the right side is the torque due to the rocker arm force. It may be noted that the number

of second order ordinary differential equation in the equation (23) is two for the rigid body variable and $2(n_1 + n_2)$ for flexible variables.

The equations of motions described above are integrated numerically with the given initial conditions and the torque, till the second joint becomes zero. At this stage the flexible link 2 locks with the link 1 and loses its rotational degree of freedom.

4. MATHEMATICAL MODEL FOR LOCKING

The first stage of locking takes place in the flexible two-link system when the angular rotation of the second joint is zero. The angular velocity of the first joint and the velocity of flexible variables after the first stage of locking is evaluated using the momentum balance method.

4.1. MOMENTUM BALANCE METHOD

The momentum balance method is based on the impulse momentum law which assumes

1. The impact occurs instantaneously and thus neglects the duration of impact.
2. The system configuration is continuous during impact and one can write

$$\mathbf{q}_- = \mathbf{q}_+. \tag{24}$$

The negative sign in the subscripts indicates the state variables just before locking and the positive sign indicates the state variables just after locking.

3. The velocities are bounded during impact.

The equation of motion for the two-link flexible system is given by

$$[\mathbf{M}]\ddot{\mathbf{q}} + \mathbf{h}(\mathbf{q}, \dot{\mathbf{q}}) + [\mathbf{K}]\mathbf{q} = \mathbf{Q}, \tag{25}$$

where

$$Q = Q_{ext} + Q_F, \tag{26}$$

with $\mathbf{Q}_{ext}$ as the generalised external forces and $\mathbf{Q}_F$ as the generalised impulsive forces due to impact.

The generalised impulsive force due to impact can be written (Greenwood [22]) as

$$\mathbf{Q}_F = F\,\mathrm{d}s/\mathrm{d}q, \tag{27}$$

where F is the impact force and s is the relative normal displacement between the impacting bodies.

Integrating over the impact period τ (i.e., $\Delta\tau = \tau_1 - \tau_2$), the equation of motion (equation (25)) yields

$$\int_{\tau_1}^{\tau_2} [\mathbf{M}]\{\ddot{\mathbf{q}}\}\,\mathrm{d}t + \int_{\tau_1}^{\tau_2} (\mathbf{h}(\mathbf{q}, \dot{\mathbf{q}}))\,\mathrm{d}t + \int_{\tau_1}^{\tau_2} [\mathbf{K}]\{\mathbf{q}\}\,\mathrm{d}t = \int_{\tau_1}^{\tau_2} \{\mathbf{Q}\}\mathrm{d}t \tag{28}$$

With the assumption that the external forces are continuous and the velocities are bounded during impact, one concludes that as the contact duration approaches zero, the integral of the two terms $\mathbf{Q}_{ext}$ and $\mathbf{h}(\mathbf{q}, \dot{\mathbf{q}})$ tends to zero. One obtains the following equations:

$$\lim_{\Delta\tau\to 0} \int_{\tau_1}^{\tau_2} [\mathbf{M}]\{\ddot{\mathbf{q}}\}\,\mathrm{d}t = [\mathbf{M}]\Delta\dot{\mathbf{q}}, \qquad \lim_{\Delta\tau\to 0} \int_{\tau_1}^{\tau_2} \mathbf{h}(\mathbf{q}, \dot{\mathbf{q}})\,\mathrm{d}t = 0,$$

$$\lim_{\Delta\tau\to 0} \int_{\tau_1}^{\tau_2} [\mathbf{K}]\{\mathbf{q}\}\,\mathrm{d}t = 0, \qquad \lim_{\Delta\tau\to 0} \int_{\tau_1}^{\tau_2} \{\mathbf{Q}_F\}\,dt = (\mathrm{d}s/\mathrm{d}\mathbf{q})\mathbf{H}, \tag{29}$$

where the generalised impulse $\mathbf{H}$ is given as

$$\mathbf{H} = \lim_{\Delta\tau \to 0} \int_{\tau_1}^{\tau_2} \mathbf{F}\, \mathrm{d}t. \tag{30}$$

The equation of momentum balance method is simplified to

$$[\mathbf{M}]\Delta\dot{\mathbf{q}} = (\mathrm{d}s/\mathrm{d}\mathbf{q})\mathbf{H}. \tag{31}$$

Hence, one can write the velocity after locking as

$$\dot{\mathbf{q}}_+ = \dot{\mathbf{q}}_- + \Delta\dot{\mathbf{q}} \tag{32}$$

The detailed equations are given in Appendix A.

5. MODELLING FOR A SINGLE FLEXIBLE LINK

The two-link flexible system described earlier locks, when the joint rotation of link 2 reaches 0°, by losing the rotational degree of freedom at joint 2. The system then reduces to a single link flexible system as shown in Figure 1d of section 2. After first locking, the two links of length l_1 and l_2 form a single link of length $(l_1 + l_2)$. The generalised co-ordinates and the velocities computed by the momentum balance method in the previous section forms the initial condition to the single flexible link system. This single flexible link now continues its rotation about the first joint. In this section, the system of equations of motion for the planar single flexible link with a revolute joint is presented. The schematic representation of the single link flexible system is shown in Figure 2(b) with the original and the deformed configurations.

The flexural deformation, v, is again approximated by the linear combination of shape functions, $\mathbf{N}$, and the nodal degrees of freedom $\mathbf{d}$ and is given by

$$v = \mathbf{N}\mathbf{d}, \tag{33}$$

where $\mathbf{d} = \{v_n, \alpha_n, v_{n+1}, \alpha_{n+1}\}^{\mathrm{T}}$, v_n and v_{n+1} are the translational nodal degrees of freedom, α_n and α_{n+1} are the rotational degrees of freedom at each node.

The total kinetic energy, the total potential energy of the single flexible link of length $(l_1 + l_2)$ and the torque due to the rocker arm at the first joint can be derived in a manner similar to the two-link flexible system described earlier. The equations of motion for a single flexible link can be written as

$$\begin{bmatrix} M_r & M_{rf} \\ M_{rf}^{\mathrm{T}} & M_f \end{bmatrix} \begin{Bmatrix} \ddot{\mathbf{p}}_r \\ \ddot{\mathbf{p}}_f \end{Bmatrix} + \begin{Bmatrix} h_r(\mathbf{p}, \dot{\mathbf{p}}) \\ h_f(\mathbf{p}, \dot{\mathbf{p}}) \end{Bmatrix} + \begin{bmatrix} K_j & 0 \\ 0 & K_f \end{bmatrix} \begin{Bmatrix} \mathbf{p}_r \\ \mathbf{p}_f \end{Bmatrix} = \begin{Bmatrix} \tau \\ 0 \end{Bmatrix}. \tag{34}$$

In the above equation, $\mathbf{p}_r$ is the joint rotation θ_{1f} and p_f are the flexible degrees of freedom of the link. It may be noted that the number of second order ordinary differential equations in equation (34) is one for the rigid body variable and $2(n_1 + n_2)$ for the flexible variables.

The equations of motion derived above are integrated numerically until the generalised co-ordinate of the first joint reaches 90°. At this stage, the first joint locks by losing its rotational degree of freedom. The single flexible link now reduces to a cantilever beam with clamped boundary condition at the first joint. The velocity of flexible variables after the second stage of locking is evaluated based on the momentum balance method. The detailed equations are given in Appendix B.

The equation of motion for the cantilever beam is given by

$$[\mathbf{M}_c]\ddot{\mathbf{p}}_1 + [\mathbf{K}_c]\mathbf{p}_1 = 0 \tag{35}$$

where $[\mathbf{M}_c]$ is the mass matrix and $[\mathbf{K}_c]$ is the stiffness matrix of the cantilever beam.

The above equations are integrated to obtain the response of the system after the second stage of locking.

6. NUMERICAL SIMULATION

The purpose of this section is to present numerical simulation results for all the three phases of the motion by accounting for the flexibility of the linkages and the effect of locking. For comparison, simulation results are also presented when the links are assumed to be rigid. The simulation is divided into three phases.

First phase: The first phase consists of the motion of each link from the initial configuration up to the first stage of locking. Link 2 locks with link 1 and hence joint 2 loses its rotational degree of freedom during first stage of locking.

Second phase: The second phase consists of the motion of the links after the first stage of locking up to the second stage of locking. In this phase the two-link flexible system rotates like a single flexible link about the first joint. During the second stage of locking the single flexible link locks and joint 1 loses its rotational degree of freedom, when it rotates through 90°.

Third phase: The third phase consists of the response after the second stage of locking. In this phase the flexible link acts like a cantilever beam.

The physical parameters of the system are presented in Tables 1–3. These are the actual values from the experimental setup. In the experimental set-up the flexural rigidity of each link is affected by the presence of flanges at the end of each link and the flexural rigidity of each components connecting the link. Hence, link 1 is stiff at both ends and link 2 is stiff at one end. The actual flexural rigidity and the equivalent cross-section for each link is arrived at, by modelling the complete region covered by the flanges and the associated components by the finite element method. The equivalent cross-section and flexural rigidity are presented in the Tables 1–3 respectively.

The numerical simulations were performed on an IBM RS6000 work station. The first order differential equations of motion were solved by a variable step, variable order (of interpolation) predictor–corrector Adams algorithm [23]. The absolute and relative errors are taken as $1{\cdot}0 \times 10^{-6}$.

First phase. The differential equations (equation (23)) are solved from the input data and the initial conditions given in Tables 1 and 2 for the first phase. Figure 3 presents the

TABLE 1

Physical parameters of link 1

Length (m)	l_1	1·006423
Cross-sectional area (m^2)	A_1	1·78076E − 4
Thickness (m)	t_1	4·4519E − 3
Area moment of inertia (m^4)	I_1	2·94113E − 10
Rotary inertia (kgm^2)	J_1	8·5948E − 4
Flexural rigidity (Nm^2)	$E_1 I_1$	20·5879
Young's modulus (N/m^2)	E_1	0·7E11
Link mass (kg)	m_1	0·52334
Tip mass (kg)	m_{p1}	1·2
Torque at joint 1 (Nm)	τ_1	0·03825
Torsion spring stiffness (joint 1) (Nm/rad)	K_1	0·0789
Prerotation angle (joint 1) (°)	θ_{01}	300·0
Initial condition (joint 1) (°)		0·0

TABLE 2

Physical parameters of link 2

Length (m)	l_2	9·945
Cross-sectional area (m^2)	A_2	1·7748E − 4
Thickness (m)	t_2	4·437E − 3
Area moment of inertia (m^4)	I_2	2·9117E − 10
Rotary inertia (kgm^2)	J_2	9·256E − 4
Flexural rigidity (Nm^2)	E_2I_2	20·3819
Young's modulus (N/m^2)	E_2	0·7E11
Link mass (kg)	m_2	0·42958
Tip mass (kg)	m_{p2}	0·336
Torque at joint 2 (Nm)	τ_2	0·0225
Torsion spring stiffness (joint 2) (Nm/rad)	K_1	0·0768
Prerotation angle (joint 2) (°)	θ_{20}	60
Initial condition (joint 2) (°)		180·0

response of joint rotations and joint velocity of each link for rigid body model and the flexible model for the first phase. The time taken by the second joint to reach zero degree for the flexible model (2·923 s) is slightly more than that of the rigid body model (2·898 s). This is because a part of energy goes into the flexible deformation of the link for the flexible model. The response of the angular velocity for the rigid body model shows a smooth and continuous variation. The response for the flexible model shows oscillatory response about the rigid body response.

Figure 4 presents the response of tip displacement and tip velocity of links 1 and 2 respectively for the first phase. The peak tip displacement for link 1 is 0·0071 m (0·705% of l_1) and for link 2 is 0·00798 m (0·845% of l_2). It is noted from Figure 3(a) that the joint rotation response for the rigid body and the flexible model are very close. This is due to a very small tip deflection of links of the flexible model during motion.

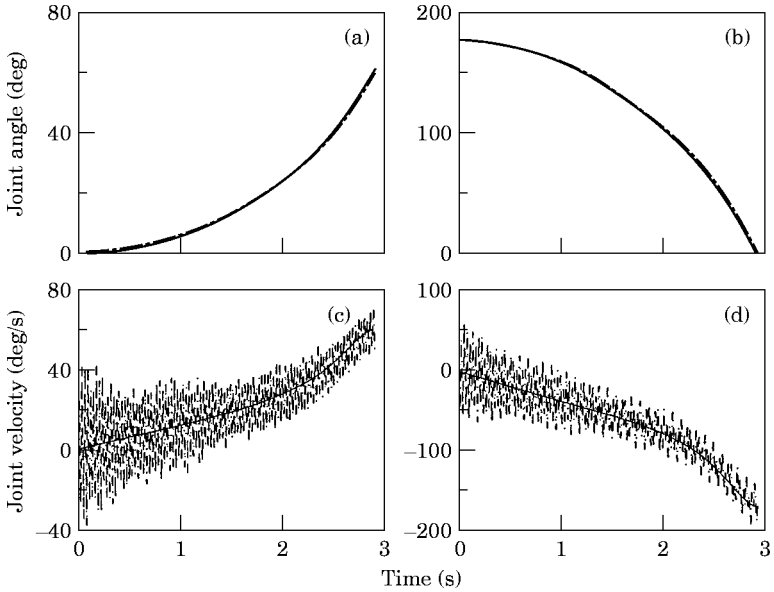

Figure 3. Response of joints during first phase. ——, rigid body model; –·–·–, flexible model; (a) joint 1; (b) joint 2; (c) joint 1; (d) joint 2.

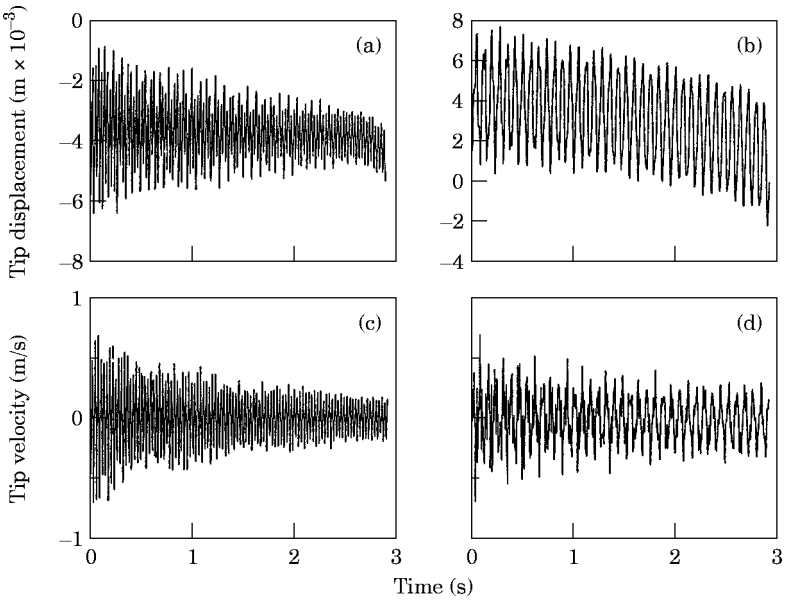

Figure 4. Response of the tip displacement and tip velocity of links during first phase. (a) link 1; (b) link 2; (c) link 1; (d) link 2.

The first stage locking takes place when joint 2 reaches 0° at 2·898 s for the rigid body model and at 2·923 s for the flexible model as mentioned above. The discontinuity in the velocities due to the first stage of locking are computed from the momentum balance method. The two link flexible system at this stage reduces to a single flexible link.

Second phase. The parameters for the second phase are presented in Table 3. The initial conditions for integrating the equations of motion are obtained from equations (31) and equation (32). The differential equations of the single flexible link (equation (34)) are solved numerically until joint 1 reaches 90°.

Figure 5 presents the response of angular rotation and angular velocity of joint 1 of single flexible link for both the rigid body model and the flexible model for the second phase. Figure 6 presents the response of tip displacement and tip velocity of the single

TABLE 3

Physical parameters of single flexible link

Length (m)	l_1	1·006423
Length (m)	l_2	0·945
Cross-sectional area (m^2)	A	1·7364E − 4
Thickness (m)	t	4·341E − 3
Area moment of inertia (m^4)	I	2·72676E − 10
Rotary inertia (kgm^2)	J_f	8·5948E − 4
Flexural rigidity (Nm^2)	EI	19·087
Young's modulus (N/m^2)	E	0·7E11
Link mass (kg)	m	0·52334
Tip mass (kg)	m_{p1}	1·2
Tip mass (kg)	m_{p2}	0·336
Torque at joint 1 (Nm)	τ_1	0·03825
Torsion spring stiffness (joint 1) (Nm/rad)	K_1	0·0789
Prerotation angle (joint 1) (°)	θ_{10}	300.0

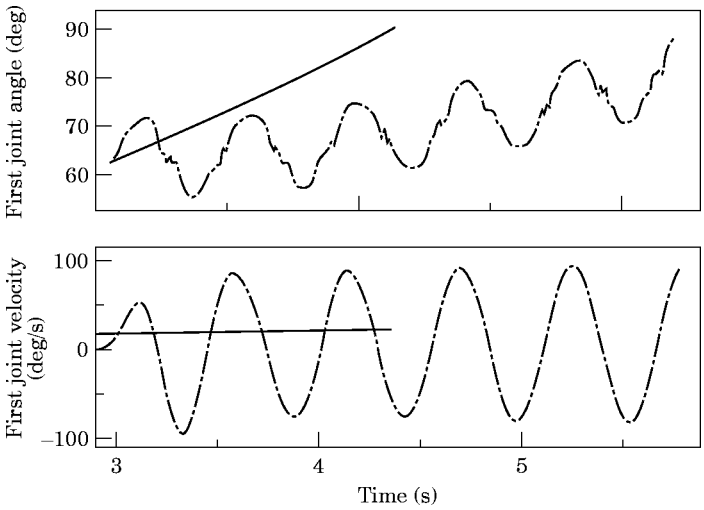

Figure 5. Response of first joint rotation and joint velocity during second phase. ——, rigid body model; –·–·–, flexible model.

flexible link for the second phase. The tip deflection is larger in comparison to the first phase. The peak tip displacement is 0·4105 m (20·5% of the total length).

For the rigid body model as a result of first locking, the kinetic energy of link 2 changes the angular velocity of the first joint by the principle of conservation of angular momentum. With this velocity as the initial condition the system rotates up to 90°. As a result of locking at the second joint, a part of the kinetic energy of link 2 is transformed into flexural strain energy and flexural kinetic energy for the flexible model. This results in an increase in tip deflection and tip velocity just after first locking. The increase in tip displacement and tip velocity of link 2 makes the joint of the single flexible link oscillate during motion. These oscillations make the flexible model take longer (5·78 s) than the rigid body model (4·38 s) to reach 90°.

It is observed from Figure 6 that the response of tip displacement contains high frequency components. This is because in the first phase two elements per link are used in the formulation. When the system locks at joint 2, the two links result in a single flexible link with four elements. This increases the dimension of the mass and stiffness matrices, which in turn introduces high frequency components. It was also observed that the tip velocity had a large number of high frequency components. This is due to the numerical problems associated with integration of the finite element based equations of motion. In the plots of tip velocity, the high frequency components have been removed by "smoothing".

The second stage of locking takes place when the first joint reaches 90°. The first joint loses its rotational degree of freedom during second locking. The discontinuity in velocity of flexible variables just after second locking is computed on the basis of the momentum balance method (equation (B1)–(B3)) of Appendix B. The single flexible link reduces to a cantilever beam with a clamped boundary condition at joint 1.

Third phase. Figure 7 presents the tip deflection and tip velocity of each link for the cantilever beam. The tip deflection of link 1 for the first phase is enhanced compared to the second phase. This enhancement is because of the rotating flexible link locks at the first joint during the second stage of locking. The peak displacement is 0·385 m (19·0% of the total length).

The comparison of the rigid body model and flexible model show that the rigid body model predicts less time for locking compared to the flexible model. Locking introduces very large deflections in the link which the rigid body model does not take into account.

7. DESCRIPTION OF EXPERIMENTAL SET-UP

In order to verify the mathematical model of the motion of a flexible linkage assembly before and after locking, an experimental study was performed. The experimental set-up is shown in Figure 8. Two flexible aluminum links are constrained to slew in the horizontal plane on top of a flat glass table. Each joint is driven by means of preloaded torsion springs made of spring steel. The first joint is supported rigidly by the side of the glass table. The second joint and the tip of the second link are floated on the glass table by means of air bearings. Each joint is provided with a locking mechanism. This prevents further rotation of the joint when the joint reaches a predefined angle.

8. DESCRIPTION OF COMPONENTS

A brief description of the main components is given below.

8.1. FLEXIBLE BEAM

Two slender aluminum beams with length 0·95 m, width 0·04 m and thickness 0·004 m, mass density 2700 kg/m^3, Young's modulus $7{\cdot}0 \times 10^{10}$ N/m^2 were selected. The beam is cantilevered on a rigid shaft and was designed to have deflection well within the elastic limit.

8.2. JOINT ASSEMBLY

The schematic representation of the joint assembly with locking mechanism for the first joint is shown in Figures 9 and 10. Figure 9 shows the initial configuration of the locking mechanism of the first joint assembly. The right flange is connected to one end

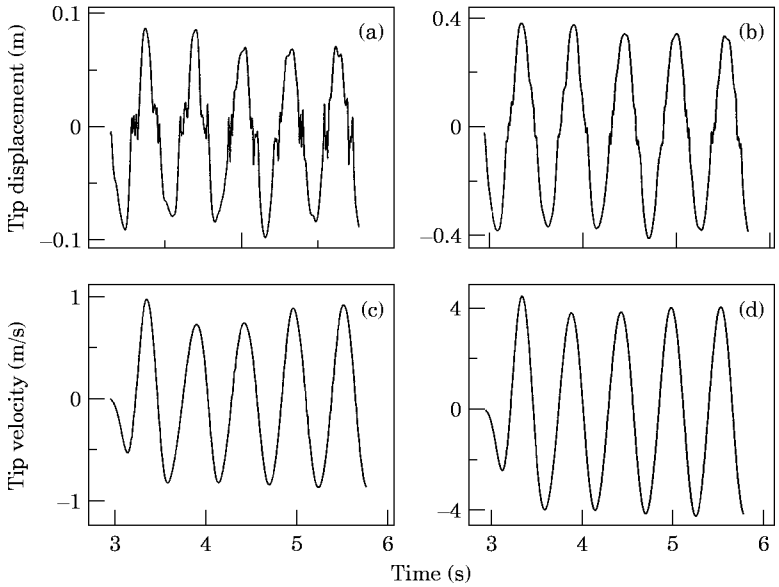

Figure 6. Response of tip displacement and tip velocity of links during second phase. (a) link 1; (b) link 2; (c) link 1; (d) link 2.

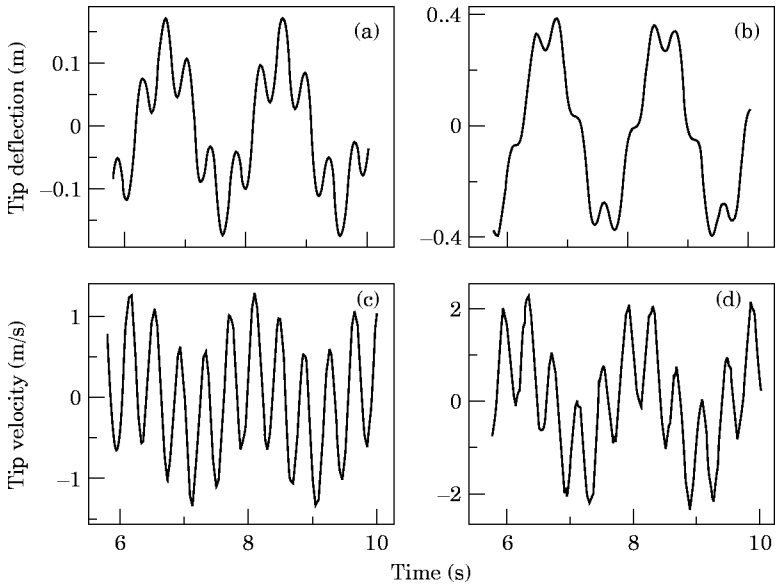

Figure 7. Response of tip displacement and tip velocity of links during third phase. (a) link 1; (b) link 2; (c) link 1; (d) link 2.

of the first link. The motion of the joint is through a pre-loaded torsion spring mounted above the right flange. The joint has a cam of circular shape and a spring loaded rocker arm. In the initial configuration the rocker arm will be resting on the surface of the cam as shown in Figure 9. During deployment the rocker arm rides over the surface of the cam. At the end of deployment the rocker arm locks with the cam due to the spring load as shown in Figure 10. This prevents further rotation of the joint. The reverse rotation of the joint after locking is prevented by projection at the other end of the cam which butts against the support block. The locking takes place when the rotation of the first joint is 90°.

A similar mechanism is designed for the second joint [21] except the locking takes place when the rotation of the second joint reaches 0°.

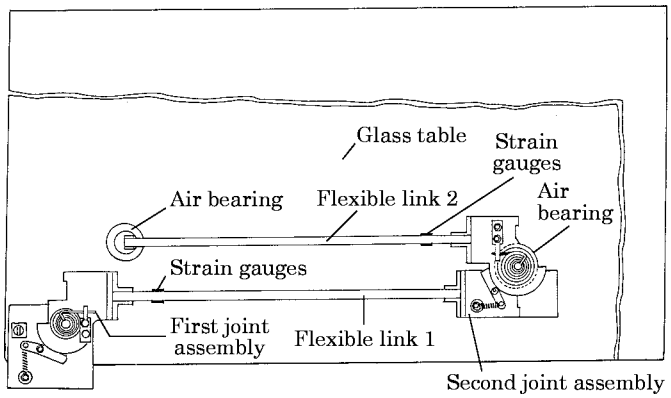

Figure 8. Experimental setup of two-link flexible system.

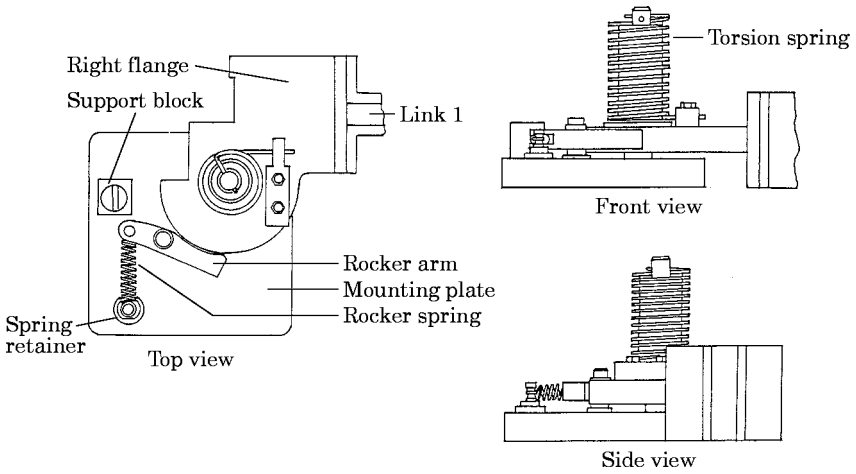

Figure 9. First joint assembly (initial configuration).

8.3. AIR BEARING

A gas lubricated bearing can be defined as two accurately machined surfaces separated by a thin film of gas and so arranged that any tendency to change the clearance between the surfaces is resisted by the change of pressure in the gas film. The bearing [24] consists of a bearing pad into which are drilled feed holes/pockets spaced evenly around the bearing circumference. Compressed air at 1·5 kgf/cm^2 from the compressor is supplied to the reservoir surrounding the bearing. The compressed air flows from the reservoir to the feed holes into the clearance between the bearing pad and the flat table. The compressed air finally exhausts to the atmosphere.

Two air bearings are used in the experimental set-up. One is mounted below the second joint assembly and the other air bearing is mounted below the tip of link 2. The compressed air is taken to the air bearing by means of light weight tubes which are taped securely to each link.

8.4. TORSION SPRINGS

The torsion spring is designed [25] for pre-rotation angles of 300° for the first joint and 240° for the second joint. The stiffness of the springs are 0·0789 Nm/rad and 0·0768 Nm/rad. The torsion spring of the first joint is right handed and rotates the link 1 in a counter clockwise direction. The torsion spring of the second joint is left-handed and rotates the link 2 in a clockwise direction.

8.5. PROVISIONS OF THE EXPERIMENTAL SET-UP

The experimental set-up can provide the variety of configurations listed below.

1. Rigid and flexible links of different cross-section or lengths can be interchanged to study the effect of structural flexibility in either or both links.
2. The width of link can be varied from 0·03 m to 0·04 m.
3. The length of each link is limited to 1 metre.
4. The torsion springs of different stiffness can be mounted on the set-up. Provision is made to vary the pre-load on the torsion spring in steps of 90°.
5. Single link experiments can be performed by dismantling the second link.

9. INSTRUMENTATION

In this section a brief description of instrumentation used in the experimental set up is described. Two types of instrumentations are used: joint angle measurement, strain measurement.

9.1. JOINT ANGLE MEASUREMENT

The rotation of each link is measured by a single turn potentiometer mounted at each joint. The resistance of each potentiometer is 10 KΩ. Each potentiometer is given an input voltage of 5 V. The output voltage of the potentiometer is recorded by a microcomputer through an A/D converter. The instrumentation block diagram is shown in Figure 11. The initial voltage of each potentiometer is noted after mounting on each joint for the initial configuration of the experimental setup. The links are moved to the final configuration and the final voltage of each potentiometer is noted. The calibration constant for each potentiometer is estimated utilizing the above recorded voltages. The results are compared with intermediate angular positions. As the potentiometer is measuring the joint rotation during motion, the system frequencies range from 35 Hz in the first phase to 1·95 Hz in the second phase and the potentiometer frequency response in this range does not pose any problem.

9.2. STRAIN MEASUREMENT

The strain at the base of each flexible link is measured using strain gauges. The gauge factor is 2·0. A full bridge circuit arrangement is used employing four strain gauges at the base of each link, two gauges on the upper and two gauges on the lower surface. The strain gauge signals are amplified 2500 times in a preamplifier. The output voltage is recorded in a microcomputer through an A/D converter. The block diagram is shown in Figure 11.

The strain measurement was calibrated statically. Each flexible link was mounted as a cantilever beam and loaded statically by a series of known weights. Measured strains were compared with the estimated strains.

10. EXPERIMENTAL RESULTS

In this section numerical simulation for the flexible model is compared with the experimental results. The comparison is made for the joint angle response, strain at

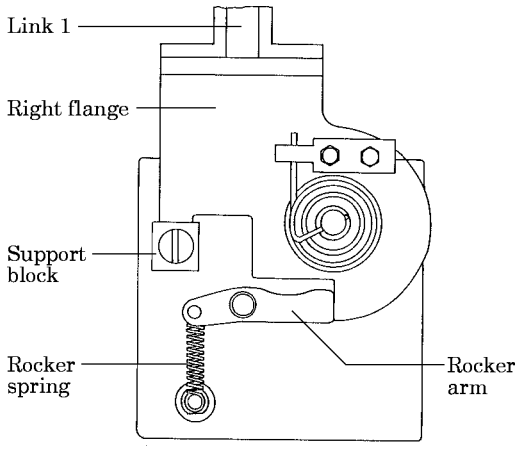

Figure 10. First joint assembly (configuration during second stage of locking).

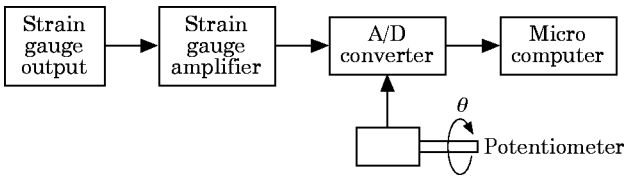

Figure 11. Instrumentation block diagram for joint rotation and strain measurement.

the base of each flexible link and finally some comments are made about the frequency of the system.

10.1. JOINT ANGLE RESPONSE

Figure 12 presents the response of joint rotations for the flexible model and the experimental results for all the phases.

First phase. The experimental results for the response of the first joint angle shows smooth and continuous variations up to the first stage of locking. The experimental results of the response of the second joint angle shows smooth and continuous variation up to the first stage of locking. It can be seen from Figure 12 that the flexible model matches very closely the experimental results in the initial stage of motion and deviates slightly at the end of the first phase. The time for the first stage of locking from the experiment is 3·07 s. This is higher than that of the flexible model, which predicts 2·923 s.

Second phase. After the first stage of locking, the experimental results for the first joint angle shows oscillatory response with slightly less amplitude compared with the flexible model. The experimental results show slightly higher time for the second stage of locking (6·13 s) than the flexible model (5·78 s). This may be due to the damping present in the experimental setup which was not modelled in the numerical simulations. Note that the response of joint 2 is not shown because it locks and does not rotate during second phase.

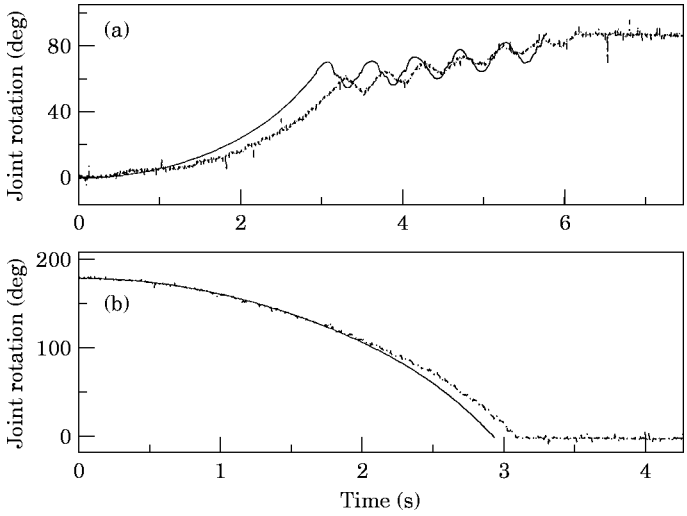

Figure 12. Response of each joint rotation for all the three phases of motion. ——, Flexible model; –·–·–, experimental data. (a) joint 1; (b) joint 2.

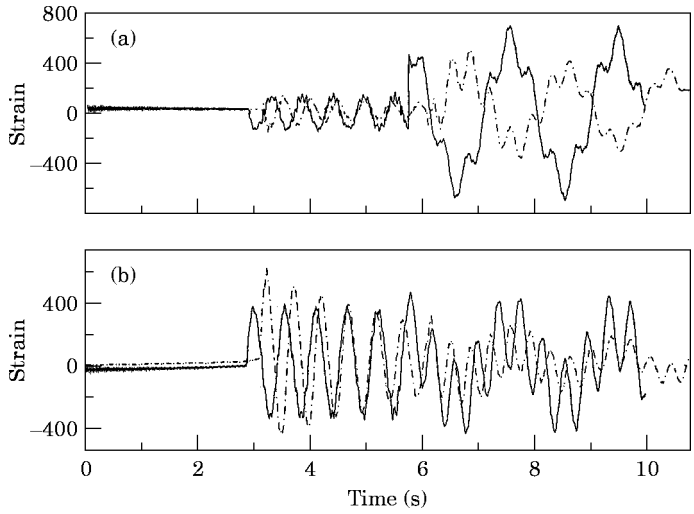

Figure 13. Response of strain in each link for all the three phases of motion. ——, Flexible model; –·–·–, Experimental data. (a) link 1; (b) link 2.

10.2. STRAIN RESPONSE

The strain at the base of each flexible link is measured by the four strain gauges. Figure 13 presents the strain response (in micro strains) for the experimental and the simulation results of the flexible model for all phases.

First phase. The strain for link 1 and link 2 up to the first stage of locking is very small. This is because the tip deflections are very small. In addition, the strain gauges and the preamplifier are not sufficiently sensitive to acquire such small values of strain. Hence, no comparison with numerical simulation are made for the first phase.

Second phase. The abrupt increase in the strain values is observed just after the first stage of locking. The magnitude of strain for link 2 is much larger than at link 1 because the locking is taking place at the second joint. The kinetic energy of link 2 just before locking is transformed to flexural strain energy and flexural kinetic energy. This induces a large strain at the base of link 2. The strain at the base of link 2 predicted by the experimental model is large compared to the flexible model for the second phase. The results of the strain of link 1 predicted by the flexible model is close to the experimental results.

After the second stage of locking, the magnitude of the strain at link 1 is larger than at link 2 because the locking is taking place at the first joint. This is again due to the kinetic energy of the combined link being transformed to flexural strain energy and flexural kinetic energy during second locking. The experimental results show a lower value of strain at link 1 and link 2 than the strain predicted by the flexible model.

It can be observed from the above figures that the increase in locking time for the first and second stages compared with the flexible model and the decrease in amplitude of strain in every cycle indicates the presence of damping. The damping arises in the experimental set-up due to friction in the joints and potentiometer shaft, structural damping of the link material and friction at the air bearings. These are difficult to estimate and were not taken into account in the numerical simulations.

10.3. FREQUENCY ANALYSIS

In this section the system frequency is evaluated from the response of the strain obtained from the flexible model and the experimental strain results by the use of Fast Fourier

Transforms (FFT). The frequency obtained from the flexible model is compared with that obtained from the experimental strain data.

After the first stage of locking (second phase of motion) the first frequency (1·95 Hz) matches quite well with the numerical model and the experimental data. This is the most dominant frequency for the flexible model as well as for the experimental results.

After the second stage of locking (third phase of motion) the first two frequencies obtained from the numerical simulation of the strain response (0·39 Hz and 2·73 Hz) is less compared to the experimental strain data (0·49 Hz and 2·93 Hz). This difference is because the exact clamped boundary condition may not happen in the experimental set-up and the stiffness of the joints and air tubes are not taken into account in simulation. After the second stage of locking the first two frequencies are dominant.

11. CONCLUDING REMARKS

A theoretical model along with an experimental set-up to study the dynamics of a two-link flexible system simulating the two panels of a solar array undergoing locking has been described in this paper. The equations of motion for the three stages of motion of the two-link flexible system are presented. The equations of motion were derived using a finite element method and the Lagrangian formulation. The model used the momentum balance method to predict the motion of the system after each locking. A comparison is made between a rigid body and the flexible model. The locking time for the rigid body model and flexible model were very close for the first stage of locking. But the locking time for the rigid body model was shown to be much smaller compared to the flexible model for the second stage of locking. Hence, a rigid body model may give inaccurate results for flexible systems which undergo locking.

In this paper, an experimental set-up consisting of two spring actuated aluminum links, floating on a glass table and undergoing locking during motion has been described. Experimental results obtained from this experimental set-up have been presented and compared with numerical simulation. The numerical simulation and the experimental results match quite well. In particular, the locking time are well matched for the first and second locking. The numerical simulation of strain response is quite close to the experimental data except at the beginning of the second phase. The frequency of the numerical simulation and the experimental strain data were compared for the second and third phases and were found to be in reasonable agreement.

The comparison of the numerical and experimental results suggest that the momentum balance method together with modelling of the flexibility of links can give reasonably accurate results. The mathematical model presented in this paper can be easily extended to model the dynamics of more than two panels. The comparison also suggests that this mathematical model can be used to predict the motion of space mechanisms which undergo locking more accurately than simple rigid body models.

ACKNOWLEDGMENTS

The authors thank M. Varadaraju of Robotics and CAD Lab, I.I.Sc and K. Vijayaprakash Rao of S M G, ISAC for useful discussions during the course of work. The authors thank M. N. Sathyanarayan, Group Director, S M G, ISAC for his encouragement and support throughout the course of this work. The authors thank M. Nageswara Rao, Group Head, S M G, ISAC and Professor A. V. Patki, Deputy Director, M S A for their continuous encouragement. Partial funding for this project was provided

by Space Technology Cell, I.I.Sc Bangalore. The authors wish to thank the anonymous reviewers for their valuable comments.

REFERENCES

1. S. Das and I. Selvaraj 1988 *Acta Astronautica* **17**, 979–986. Solar array mechanism for Indian satellites, APPLE, IRS and INSAT-II TS.
2. P. E. Gauitier and W. L. Cleghorn 1992 *Mechanism and Machine Theory* **27**, 415–433. A spatially translating and rotating beam element for modelling flexible manipulators.
3. J. Bricout, J. C. Dedus and P. Michean 1990 *Mechanisms and Machine Theory* **25**, 119–128. A finite element model for the dynamics of flexible manipulators.
4. P. B. Usoro, B. Nadira and S. S. Mahil 1986 *ASME Journal of Dynamic Systems*, *Measurement and Control* **108**, 198–205. A finite element/Lagrange approach to modelling light weight flexible manipulators.
5. R. J. Theodore and A. Ghosal 1995 *The International Journal of Robotics Research* **14**, 91–111. Comparison of assumed mode and finite element method for flexible multilink manipulators.
6. W. J. Book 1987 *The International Journal of Robotics Research* **3**, 87–101. Recursive Lagrangian dynamics flexible manipulator arm.
7. G. Hastings and W. J. Book 1987 *IEEE Control System Magazine* **7**, 61–64. Linear dynamic model for flexible link manipulator.
8. Alessandro de Luca 1991 *IEEE Transactions on Systems Man and Cybernetics* **21**, 826–839. Closed form dynamic model planar multilink weight robots.
9. Y. Wang and R. L. Huston 1994 *Computers and Structures* **50**, 421–432. A lumped parameter method in the nonlinear analysis of flexible multibody systems.
10. B. Wie, N. Furumoto, A. K. Banerjee and P. M. Barba 1986 *AIAA Journal of Guidance Control and Dynamics* **9**, 593–598. Modelling and simulation of spacecraft solar array deployment.
11. B. S. Nataraju and A. Vidyasagar 1987 38*th Congress of IAF*, *Brighton*, *England*. Deployment dynamics of accordion type of deployable solar arrays considering flexibility of closed control loops.
12. Y. A. Khulief and A. A. Shabana 1986 *ASME Journal of Mechanism*, *Transmission and Automation in Design* **108**, 38–45. Dynamic analysis of a constrained system of rigid and flexible bodies with intermittent motion.
13. Y. A. Khulief and A. A. Shabana 1986 *ASME Journal of Mechanisms*, *Transmission and Automation in Design* **108**, 167–175. Dynamic of multibody systems with variable kinematic structure.
14. J. Rismantab-sany and A. A. Shabana 1990 *ASME Journal of Vibration and Acoustics* **112**, 119–126. On the use of momentum balance in the impact analysis of constrained elastic systems.
15. A. S. Yigit, A. G. Ulsoy and R. A. Scott 1990 *ASME Journal of Vibration and Acoustics* **112**, 65–70. Dynamics of a radially rotating beam with impact, Part 1: theoretical and computational model.
16. A. S. Yigit, A. G. Ulsoy and R. A. Scott 1990 *ASME Journal of Vibration and Acoustics* **112**, 71–77. Dynamics of a radially rotating beam with impact, Part 2: experimental and simulation results.
17. A. S. Yigit, A. G. Ulsoy and R. A. Scott 1990 *Journal of Sound and Vibration* **142**, 515–525. Spring–dashpot models for the dynamics of a radially rotating beam with impact.
18. B. V. Chapnik, G. R. Heppler and J. D. Aplevich 1991 *IEEE Transactions on Robotics and Automation* **7**, 479–488. Modelling impact on a one link flexible robotic arm.
19. A. S. Yigit 1994 *Journal of Sound and Vibration* **177**, 349–361. The effect of flexibility on the impact response of a two-link rigid flexible manipulator.
20. S. S. Rao 1989 *Finite Element Method in Engineering*. Oxford: Pergamon; second edition.
21. B. P. Nagaraj 1996 *M.Sc. Eng. Thesis*, *Department of Mechanical Engineering*, *Indian Institute of Science*, *Bangalore*, *India*. Dynamics of two link flexible systems: modelling and experiments.
22. D. T. Greenwood 1977 *Classical Dynamics*. Eaglewood Cliffs: Prentice Hall.
23. L. F. Shampine and M. K. Gordon 1975 *Computer Solution of Ordinary Differential Equations*: *the Initial Value Problem*. San Francisco: W. H. Freeman.
24. J. W. Powell 1970 *Design of Aerostatic Bearings*. London: The Machinery Publishing Company.
25. H. Carlson 1978 *Spring Designers Handbook*. New York: Marcel Dekker.

APPENDIX A: MOMENTUM BALANCE FOR THE FIRST STAGE OF LOCKING

The elements of mass matrix [**M**] for the flexible two-link system given in section 3 (equation (23)) can be written as

$$[\mathbf{M}_r] = [M_{r1}, M_{r2}], \qquad [\mathbf{M}_{rf}] = [M_{rf1}, M_{rf2}]^{\mathrm{T}}. \tag{A1}$$

The equation of momentum balance method for the flexible two-link system undergoing locking at the second joint is given by

$$[\mathbf{B}_1]\Delta\dot{\mathbf{S}}_1 = \mathbf{F}_1, \tag{A2}$$

where

$$[\mathbf{B}_1] = \begin{bmatrix} M_{r1} & M_{rf} & h_1 \\ M_{rf_1}^{\mathrm{T}} & M_f & h_2 \end{bmatrix}, \qquad \mathbf{h}_1 = \{0, -1\}^{\mathrm{T}}, \qquad \mathbf{h}_2 = \{0\}^{\mathrm{T}},$$

$$\Delta\dot{\mathbf{S}}_1 = \{\Delta\dot{\theta}_1, \Delta\dot{\mathbf{q}}_1, \Delta\dot{\mathbf{q}}_2, H_1\}^{\mathrm{T}}, \qquad \mathbf{F}_1 = \{-\Delta\dot{\theta}_2\, M_{r2}^{\mathrm{T}}, -\Delta\dot{\theta}_2\, M_{rf2}\}^{\mathrm{T}}. \tag{A3}$$

In the above equation H_1 is the impulse acting at the joint 2 and $\dot{\theta}_{2+} = 0$ due to locking at joint 2.

APPENDIX B: MOMENTUM BALANCE FOR SECOND STAGE OF LOCKING

The equation of momentum balance method for the flexible one-link system undergoing locking at the first joint is given by

$$[\mathbf{B}_2]\Delta\dot{\mathbf{S}}_2 = \mathbf{F}_2, \tag{B1}$$

where

$$[\mathbf{B}_2] = \begin{bmatrix} M_{rf} & h_1 \\ M_f & h_2 \end{bmatrix}, \qquad \Delta\dot{\mathbf{S}}_2 = \{\Delta\dot{p}_1, H_2\}^{\mathrm{T}}, \qquad \mathbf{F}_2 = \{-\Delta\dot{\theta}_1\, M_r, -\Delta\dot{\theta}_1\, M_{rf}\}^{\mathrm{T}} \tag{B2}$$

In the above equation, the terms M_r, M_{rf} and M_f of $\mathbf{B}_2$ and $\mathbf{F}_2$ are the elements of mass matrix of the equation (34), $h_1 = -1$, $h_2 = \{\mathbf{0}\}$, H_2 is the impulse acting at the joint 1 and $\dot{\theta}_{1+} = 0$ due to locking to joint 1.

The velocity of the flexible variables, $\dot{\mathbf{p}}_{1+}$, just after locking is given by

$$\dot{\mathbf{p}}_{1+} = \dot{\mathbf{p}}_{1-} + \Delta\dot{\mathbf{p}}_1, \tag{B3}$$

where $\dot{p}_{1-}$ are the velocities of flexible variables just before locking and $\Delta\dot{\mathbf{p}}_1$ are the changes in velocities of flexible variables due to locking.